

LONDON, METEOROLOGICAL OFFICE  
Met.O.15 Internal Report No. 68

Interpretation of satellite imagery using  
diagnostics from numerical forecast models: a  
case study.

06620886

FH58

FGZ

**National Meteorological Library  
and Archive**

Archive copy - reference only



279

METEOROLOGICAL OFFICE  
London Road, Bracknell, Berks.

METEOROLOGICAL OFFICE

148653

LIBRARY

# MET.O.15 INTERNAL REPORT

No 68

INTERPRETATION OF SATELLITE IMAGERY USING DIAGNOSTICS  
FROM NUMERICAL FORECAST MODELS: A CASE STUDY

by

M V YOUNG Met Office Bracknell

V ZWATZ-MEISE, Institute of Meteorology and Geodynamics, Vienna

Cloud Physics Branch (Met.O.15)  
August 1986



INTERPRETATION OF SATELLITE IMAGERY USING DIAGNOSTICS FROM NUMERICAL  
FORECAST MODELS: A CASE STUDY

by M V Young, Meteorological Office, Bracknell

and V Zwatz-Meise, Institute of Meteorology and Geodynamics, Vienna

CONTENTS

1. Introduction
2. Dynamical interpretation and frontal analysis of features on infra-red imagery.
  - 2.1 The parameters used for interpretation.
  - 2.2 Application of the parameters to this case study.
  - 2.3 Discussion.



3. Use of satellite water vapour imagery and numerical model diagnostics relating to cyclogenesis.

3.1 The basic principles.

3.2 Dynamical significance of the dry zones seen on water vapour imagery on 11 April 1985.

3.3 Discussion.

4. Influence of the dry tongue on the mesoscale features, following cyclogenesis.

5. Conclusions.



## 1. Introduction

Forecasts up to a day ahead are made using guidance from numerical forecast models (see eg Woodroffe, 1984). Satellite imagery, if exploited to the full can provide very valuable complementary information for sharpening up conventional analyses, identifying mesoscale features, and extrapolating system movement. A further application of imagery is in refining model products; that is, inferring variations in 'weather', and signalling when the model's predicted evolution is likely to be incorrect.

The aim of this paper is to show, using the case study described in Paper I (Monk, 1986), how satellite imagery can be interpreted more fully using non-routine diagnostics from numerical models in terms of

- i. Dynamics and frontal analysis.
- ii. Predicting cyclogenesis and
- iii. Explaining the observed mesoscale features described in Paper I.



## 2. Dynamical interpretation and frontal analysis of features on infra-red imagery

### 2.1 The parameters used for interpretation

A sequence of infra-red pictures from METEOSAT is compared with various parameters computed on standard pressure levels from analyses of the numerical model used by the European Centre for Medium Range Weather Forecasts (ECMWF). The parameters are used to highlight the synoptic and dynamical significance of the features seen on the imagery. The grid length of the model is 1.875 degrees of latitude and longitude.

In particular, parameters applied operationally in the Institute of Meteorology and Geodynamics, Vienna, (Zwatz-Meise 1983) as an aid to analysis and short period forecasting will be demonstrated. They are

(i) Thermal advection in the layer 850/500 mb.

(ii) Relative vorticity and positive vorticity advection (PVA) at 500 mb.

These two quantities are chosen because they represent two terms in the 'Omega' equation describing vertical motion (see eg Morris, 1971). PVA and warm air advection (WA) imply ascent, whilst negative vorticity advection and cold advection (CA) both imply descent.



(iii) Thermal front parameter (TFP) of the 850/500 mb layer. TFP is used for identifying whether or not a feature on the imagery is frontal. It is simply the change in thickness gradient in the direction of the thickness gradient, and its mathematical derivation is shown in Huber-Pock and Kress (1981). The front is assumed to lie along the maximum of TFP which (in common with conventional analysis procedures) lies on the warm side of the thermal gradient. If a cloud band coincides with a TFP maximum, it is assumed to be frontal. Examples of its application are given in Zwatz-Meise (1983).

## 2.2 Application of the parameters to this case study

The parameters are illustrated in Figs. 1-4, for 00, 06 and 12 GMT on 11 April 1985, superimposed on a schematic representation of the main areas of cold cloud ( $\leq -30^{\circ}\text{C}$ ) derived from METEOSAT infra-red imagery at the same times. NOAA satellite pictures showing the principal cloud areas are clearly shown in Paper I, Fig. 1.

The evolution of three main cloud areas: R, 1, and D are described. Initially the pattern is somewhat disorganised. However, in the next 12 hours, area 1 becomes a well marked band with a distinct rear edge as it moves south-east. Cloud area D decays rapidly after 00 GMT whilst R becomes a well marked convective feature as discussed in Paper I.



(a) Thermal advection (Figure 1)

The thermal advection fields show, in the 12 hour period,

(i) A large area of WA corresponding closely with the layered cloud area 1 which persists and produces widespread moderate rain.

(ii) CA behind area 1 and near D which dissipates.

The behaviour of these cloud areas is therefore consistent qualitatively with the vertical velocity fields in Fig. 5 and also with the inferences from the parameters: WA giving rise to ascent and CA giving rise to descent.

Between the two areas of advection, a cloud edge emerges corresponding to the 'upper cold front' described in Paper I.

b. Vorticity fields (Figures 2 and 3)

Figure 2a shows that at 00 GMT, cloud signature R lies immediately ahead of a vorticity maximum within a region of strong PVA. This leads to ascent as shown in Figure 5. At 1200 GMT, by which time the vorticity maximum had intensified, R has become organised into a 'comma' - a shape often associated



with PVA (eg Anderson et al 1973). (R also lies within the CA region - favouring descent - but the persistence and increased organisation of the cloud implies that the PVA term dominates).

Successive analyses or forecasts of upper level vorticity or PVA may well be of practical use to a forecaster. A well marked maximum of either should alert the forecaster to the possibility of organised deep convection even if none is apparent on the latest imagery. Conversely, a well marked convective comma on imagery implies presence of a vorticity maximum aloft, and such information may be used to modify machine analyses in data sparse areas.

c. Thermal Front Parameter (TFP) (Figure 4)

The TFP at 00 GMT (Figure 4a) highlights two frontal zones. The northern one passes through a rather complex area of cloud encompassing D but clearly ahead of R. The portion of the TFP over Ireland corresponds well with the surface cold front (Figure 2b of Paper I). In the next 12 hours (Figures 4b and 4c), the TFP moves quickly eastwards. It approaches the rear of cloud band 1 and its position continues to correspond closely with the surface cold front. The correspondence of the TFP with cloud band 1 shows that the cloud is frontal and the front itself is close to the rear edge. However, the model's grid length puts a



limit on the precision with which the front can be located and it is not possible to distinguish between the upper and surface frontal positions as described in Paper I.

The southern front location, defined by the TFP at 00 GMT on the 11th April 1985 compares well with the analysis of a surface warm front (Figure 2b of Paper I). By 06 GMT, however, no TFP can be resolved, suggesting that the front aloft has become thermally insignificant. It may be hypothesized that area 1 results from ascent due to WA.

The advantages to the forecaster of the TFP are that it provides useful objective guidance:

(i) of frontal location, especially in data sparse areas, as shown in this case study.

(ii) where boundary layer effects mask the commonly accepted surface frontal criteria for example over continental areas in wintertime, or over mountains.

d. Inferences from combining the parameters

It is often useful to examine the imagery with more than one parameter. This case shows an example. Figures 4a to c show that cloud area R catches up with the northern TFP, and by 12 GMT on 11th April, they nearly coincide, implying that R takes over



the role of the cold front. This is supported by the 12 GMT observations (Paper I) showing that the trough associated with R has marked cold frontal characteristics: a marked drop in  $\theta_w$ , a band of heavy rain, a sharp wind veer and rise of pressure - and are much more prominent than on the original cold front. This example shows that the PVA feature behind a cold front can become a dominant feature responsible for apparent delayed cold front clearance, and should be looked for in the imagery.

### 2.3 Discussion

The application of the parameters, as described in Section 2.2, may appear to be very subjective. Indeed, subjectivity is the essence of such methods because they are intended to provide a simple and quick way of focussing on features of the imagery to help the forecaster to clarify his ideas on the analysis, and understand the likely evolution of cloud patterns. Some of the patterns may be self-contained and readily identifiable. When they are complex and amorphous the parameters may help the forecaster to disentangle the message the imagery portrays.

The method has the big advantage of being able to focus on particular signatures and is intended to complement conventional forecasting techniques which use numerical data fed into models that cannot recognise patterns as such. Inferences made from imagery may sometimes form a sound basis for model intervention when, for



instance, the numerical model is not thought to be handling a particular feature very well, perhaps because of a developing system in a data sparse area.

The potential operational applicability of such methods in forecasting depends on the repeatability of cloud signatures associated with particular dynamical quantities and is being investigated through further case studies.

### 3. Use of Satellite Water Vapour Imagery and Numerical Model Diagnostics Relating to Cyclogenesis

#### 3.1 The basic principles

In Section 2, infra-red imagery and certain dynamical parameters have provided evidence of probable cyclogenesis. In this section, an alternative method is described for explaining the sequence of events leading to cyclogenesis using imagery from a different channel and another parameter whose significance has recently been brought to the fore.

Instead of following the cloud features from the infra-red images, we concentrate here on the 'water vapour imagery' described in Section 3 of Paper 1. It provides a measure of moisture in the upper troposphere, normally between 300 and 600 mb (Eyre, 1981) and is



particularly useful for describing large scale mid and high tropospheric circulations. The feature of this case is the marked intrusion of dry air shown in this channel.

Such 'dry intrusions' (eg Young et al, 1986) can be related to the parameter called 'isentropic potential vorticity' (IPV) which has the advantage that it combines, into one quantity, the components in the omega equation describing the ascent and descent of air. For a full appraisal of IPV, the reader is referred to Hoskins et al (1985).

The main practical applications of IPV are based on the fact that

(i) Air with high IPV descends from the lower stratosphere and is therefore very dry, so the dry intrusions can be seen on the water vapour imagery and are therefore related to high IPV.

(ii) At the leading edge of the high IPV tongues, ascent of air is favoured through advection of IPV. (According to the Hoskins et al, there is a strong case for permitting the acronym, PVA, to be read as (positive) 'potential vorticity advection')

The presence of these rapidly moving dry tongues seen on the water vapour imagery should therefore alert the forecaster to possible cyclogenesis particularly when, according to Hoskins et al, the leading edge of the dry air over-runs low level baroclinicity. This case study clearly illustrates the application of the principles. The



presence of the dry air also has a profound influence upon the mesoscale distribution of cloud and precipitation and will be described in Section 4.

### 3.2 The dynamical significance of the dry zones seen on water vapour imagery on 11th April 1985

IPV was computed from forecasts by the Meteorological Office fine mesh model at 6 hourly intervals, based on data received at 12 GMT on 10 April. The period chosen for investigation was 18 GMT on 10th to 12 GMT on the 11th, covering the period of the cyclogenesis (Figure 4 of Paper I). Forecasts rather than analyses were used because fields were available every 6 hours instead of every 12; thus the evolution of the main weather features could be followed at more frequent intervals giving a more sound time continuity.

It was possible to use model forecasts to follow the evolution because the model handled the case very well, particularly at upper levels as demonstrated in Figure 6. Furthermore, the observed shape and extent of the dry intrusion was well reproduced by the humidity mixing ratio field computed on the 310°K surface (Figure 7) north of the jet axis. From 00 GMT to 12 GMT on 11th April the sharp forward edge of the dry intrusion observed in the water vapour imagery corresponded closely to the  $0.1 \text{ g kg}^{-1}$  humidity mixing ratio contour, showing the expected agreement of what is a conserved quantity (in the absence of mixing).



Maps of IPV calculated on the  $\theta = 315^\circ\text{K}$  surface from the fine mesh model are shown in Figures 8a to d at 6 hourly intervals between 18 GMT on 10th and 12 GMT on the 11th. The  $315^\circ\text{K}$  surface was chosen because it intersected the dry intrusion and was representative of the air in the jet stream (Figure 6) with which the dry intrusion was associated. A tongue of high IPV labelled S, initially north of latitude  $55^\circ\text{N}$  advects east southeastwards towards the UK. Values within the tongue exceed 4 units, thought by Hoskins et al to originate from the stratosphere. These descend to as low as 420 mb (by inspection of lower isentropic surfaces).

The water vapour imagery was not available over the western and mid-Atlantic. However, we may hypothesize that the air with high IPV correlates with the observed dry intrusion; indeed, by comparing Figure 3b of Paper I with Figure 8c, the forward edge of both are over the western UK by 0600 GMT on the 11th.

In an attempt to show the relationship between IPV (and hence the observed dry intrusion) and cyclogenesis, IPV contours derived from the fine mesh model analyses have been superimposed (Figure 9) with the surface synoptic charts at 12 hourly intervals, along with the observed cloud outlines (from the infra-red imagery) and the jet axis. Although at 12 GMT on the 10th the jet extends towards the British Isles in association with the extensive cirrus shield, the major region of high IPV (containing values of  $\geq 6$  in Figure 9a) lies well upstream. When, after 00 GMT on the 11th, the jet stream and its accompanying high IPV meets the frontal zone, and in particular the



surface wave X, cyclogenesis commences and becomes rapid (see Figure 4 of Paper I), the largest pressure falls being at the leading edge of the dry tongue (Figure 3 of Paper I). This example clearly supports the theoretical ideas of Hoskins et al that cyclogenesis is favoured when the leading edge of a high IPV tongue over-runs a low-level baroclinic zone.

### 3.3 Discussion

The main advantages of identifying and following dry intrusions on water vapour imagery are as follows:

(i) Dry intrusions stand out very clearly.

(ii) The location of dry intrusions corresponding to tongues of high IPV help in identifying likely cyclogenesis. It is interesting to note that in other cases (eg Uccellini et al 1985, Young et al 1986), rapid cyclogenesis was also accompanied by marked dry tongues on the water vapour imagery which were apparent 12 to 24 hours earlier. In both cases the accompanying stratospheric air could be traced on successive IPV analyses and as it approached the frontal zone, rapid cyclogenesis commenced. The appearance on water vapour imagery of an anomalously dry area adjacent to a jet streak (ie a wind maximum within a jet stream) which then elongates into a dry intrusion should be noted by the forecaster, especially when it approaches a pre-existing frontal zone. Such observations may provide valuable additional



information on the likely timing and location of cyclogenesis which may support or go against conventional operational guidance. (further evidence of cyclogenesis or deepening may be inferred from the imagery by the development of deep convection near the depression centre. This occurred over northern England on 11th April).

(iii) A feature of dry intrusions and IPV maps is the degree of continuity in both shape and motion of the features over many hours. In this case and in other cases (eg Gurka, 1985), a depression moved in a direction similar to the main thrust of the forward edge of the dry intrusion observed in a movie loop of water vapour images. The track of depressions can therefore be predicted by extrapolation for several hours ahead with some confidence.

#### 4. The influence of the dry tongue on the mesoscale features, during cyclogenesis

Portions of the cloud and moisture patterns on the satellite imagery have so far been attributed to large scale advection fields. In this section, a three dimensional conceptual model describing the mesoscale structure early in the cyclogenetic phase - described in Paper I - will be given. The basis of the conceptual model will be the dry intrusion, whose properties will be discussed first. The influence of the dry intrusion on the mesoscale then follows.



As a simplified alternative to trajectories, air motion is computed along an isentropic surface -  $310^{\circ}\text{K}$  - relative to the movement of the dry intrusion's leading edge ( $275^{\circ}/35 \text{ ms}^{-1}$ ). The air flow is based on the fine mesh analysis for 00 GMT on 11 April; the principles of the method are described in Green et al (1966).

The airflow within the dry intrusion is shown in Figure 10. The sense of the vertical motion is broadly consistent with Figure 5. South of the jet axis the air descends, slowly at first but then more rapidly as it turns anticyclonically. North of the jet, the air also descends but as it approaches the western UK it ascends and turns cyclonically. These two different flows have an important bearing on the mesoscale.

Figure 11 shows a conceptual model of the cyclone, immediately prior to cyclogenesis, the dry air flows being those of Figure 10. The northern portion contains the downward extrusion of the stratospheric air, inferred from the IPV treatment. The forward edge of this flow eventually forms the dry slot of the developing depression that can be seen on the water vapour imagery over central England in Figure 3d of Paper I. This air over-runs warm air at low levels during the morning of 11th April, generating potential instability. The overall ascent at the leading edge of the dry tongue (as inferred by relating it with the IPV anomaly) allowed the instability to be released, producing the heavy rain over Wales and northern England described in Paper I, Section 5, as well as along the UCF. Additionally, ascent of air in this region also allowed cloud area R to develop (Fig. 9b) - in this case into a well organised, active convective trough.



The southern portion contains subsiding air near the right hand exit of the jet, resulting in rapid dispersal of the pre-existing upper cloud (eg cloud area D in Figure 1) leaving the dry cloud free air overlying a shallow layer of low cloud in the warm sector; the 'shallow moist zone'. This process leads to the formation of the 'split front' consisting of the sharp upper cold front (and onset of cold advection in the 850-500 mb layer) at the head of the dry intrusion, and the surface cold front further west at the rear of the shallow moist zone.

The features shown in the conceptual model - in particular the dry intrusion and split front - occur in many cyclogenesis events and are responsible for the commonly observed sequence of weather events described in Paper I.

## 5. Conclusions

The particularly instructive and clear cut case study of cyclogenesis on 11th April 1985 has suggested ways in which the forecaster may fully exploit the messages portrayed by features on the satellite imagery, with the help of diagnostics from numerical forecast models.

Features on the imagery have been interpreted in terms of the dynamics, and frontal analyses have been improved, especially in data sparse areas. The importance of the dry intrusion, clearly identified on the water vapour imagery, has been shown in relation to



(i) the onset of cyclogenesis, supported by the theoretical ideas on isentropic potential vorticity (IPV).

(ii) Forecasting depression tracks.

(iii) Explaining the commonly observed mesoscale weather - especially the split front - in terms of a conceptual airflow model.

The concepts discussed above should help the forecaster with his analysis, understanding and prediction of weather associated with cyclogenesis and split fronts, and with assessing the validity of conventional products from operational numerical forecast models. The generality of the concepts need to be confirmed by carrying out further case studies, the results of which will form Paper III.



## Figure Legends

Figure 1. Comparison between upper cloud areas (stippled) and thermal advection for (a) 00 GMT, (b) 06 GMT, (c) 12 GMT 11th April 1985. The line of zero thermal advection is dashed. Areas undergoing warm advection are labelled WA, whilst areas of cold advection are labelled CA. The labels WA and CA are located in the maximum of their respective advection fields. Cloud areas R, 1, and D are those referred to in the text. Upper cloud areas have been derived from METEOSAT infra-red imagery and are those areas with cloud tops colder than  $-30^{\circ}\text{C}$ .

Figure 2. Upper cloud areas (defined as in Figure 1) and 500 mb relative vorticity (continuous lines) for (a) 00 GMT, (b) 06 GMT, (c) 12 GMT 11th April 1985. Relative vorticity is shown for values greater than or equal to zero and is expressed in units of  $10^{-5}\text{s}^{-1}$ .

Figure 3. Upper cloud areas (defined as in Figure 1) and 500 mb positive vorticity advection (PVA), for (a) 00 GMT, (b) 12 GMT 11th April 1985. PVA is shown as continuous lines for values greater than or equal to zero and is expressed in units of  $10^{-9}\text{s}^{-2}$ .



Figure 4. Upper cloud areas (defined as in Figure 1) and thermal front parameter (continuous bold lines) for the 850/500 mb layer for (a) 00 GMT, (b) 06 GMT, (c) 12 GMT 11th April 1985.

Figure 5. 600 mb vertical velocity in  $\text{cms}^{-1}$  derived from a fine mesh analysis for 00 GMT 11th April 1985 superimposed over observed upper cloud areas (stippled). Areas of upward motion greater than  $4 \text{ cms}^{-1}$  are heavily stippled, and areas of downward motion greater than  $4 \text{ cms}^{-1}$  are hatched. The cloud area is defined as in Figure 1a, and R, D and 1, are located in the cloud areas referred to in the text.

Figure 6 300 mb charts for 12 GMT 11th April 1985. (a) is an analysis reconstructed by the authors using the fine mesh analysis and observational data. (b) is a 24-hour fine mesh forecast. Dashed lines are isotachs greater than 60 knots and values in excess of 140 kts are stippled. Jet axes are marked with bold arrows. Actual wind reports are shown in Figure 6a. Notice how the location of the upper trough and the strong northwesterly flow into Biscay are well represented by the model's forecast.

Figure 7. 18 hour forecast of humidity mixing ratio and jet location on the  $\theta = 310^\circ\text{K}$  surface. Dry areas (with mixing ratio less than  $0.07 \text{ gkg}^{-1}$ ) are stippled, demonstrating the dry tongue lying north of the jet axis. The jet axis is shown by the bold arrow and corresponds to the axis of maximum wind in



excess of 100 knots on the 310°K surface. The forward limit of dry air near the UK at 06 GMT 11th April as observed by water vapour imagery is represented by a dashed line.

Figure 8. 6, 12, 18, and 24 hour forecasts of isentropic potential vorticity (IPV) on the 315°K surface derived from the fine mesh, valid at (a) 18 GMT 10th April 1985, (b) 00 GMT 11th April 1985, (c) 06 GMT 11th April 1985, (d) 12 GMT 11th April 1985. IPV is defined as

$$g \frac{\partial \theta}{\partial p} (\xi_\theta + f)$$

and expressed in units of  $10^{-6} \text{m}^2 \text{s}^{-1} \text{Kkg}^{-1}$  suggested by Hoskins et al (1985). Stratospheric air, characterised by values in excess of 4 units is stippled. 'S' denotes the region of high IPV thought to be associated with the cyclogenesis.

Figure 9. Surface charts, upper cloud areas (stippled), jet axis, and IPV contours for (a) 12 GMT 10th April 1985, (b) 00 GMT 11th April 1985, (c) 12 GMT 11th April 1985. The jet axis and IPV contours are calculated on the 315°K surface, the jet being the bold arrow denoting winds of over 100 knots. IPV contours of 4 and 6 units are dashed, areas greater than 4 being hatched. These are derived from model analyses valid at the above times in order to be directly compatible with the synoptic charts. Cloud areas are derived from



available NOAA and METEOSAT imagery and correspond to tops colder than  $-30^{\circ}\text{C}$ . X is the wave on which rapid cyclogenesis occurred. R is the cloud mass referred to in the text, lying in the region where advection of IPV is large.

Figure 10. Relative flow analyses on the  $\theta = 310^{\circ}\text{K}$  surface derived from a fine mesh analysis for 00 GMT 11th April 1985. The continuous lines are streamlines calculated relative to a system velocity of  $275^{\circ}/50$  kts. Pecked lines show the pressure level in millibars of the  $\theta = 310^{\circ}\text{K}$  surface. The circled plus and minus signs indicate the sense of the implied vertical motion in the places shown, plus representing upward, and minus representing downward motion. The stippling bounded by the cusped line represents the limit of moist air on the  $\theta = 310^{\circ}\text{K}$  surface.

Figure 11. Conceptual model of the dry intrusion appropriate to 00 GMT 11th April 1985. The broad hatched arrows represent the relative flows on the  $\theta = 310^{\circ}\text{K}$  surface shown in Figure 10. This mostly subsiding flow of dry air comprises the dry intrusion. The line of zero thermal advection is dashed and areas of warm and cold advection are labelled WA and CA respectively. Surface fronts are shown by the conventional symbols and the cold front wave which underwent cyclogenesis is labelled X. The upper level cloud outline, defined as in Figure 1a is shown by stippling.



## References

- Anderson, R K, and Veltishchev, N F 1973 The use of satellite pictures in weather analysis and forecasting. WMO Tech. Note No. 124.
- Eyre, J R 1981 METEOSAT water vapour imagery. Met. Mag., 110, 345-351.
- Green, J S A, Ludlam, F H, and McIlveen, J F R 1966 Isentropic relative flow analysis and the parcel theory. Quart. J. R. Met. Soc., 92, 210-219.
- Gurka, J J 1985 The use of 6.7 micron water vapour imagery for improving precipitation forecasts. Amer. Met. Soc., 6th Conf. Hydromet. pp 260-265.
- Hoskins, B J, McIntyre, M E, and Robertson, A W 1985 On the use and significance of isentropic potential vorticity maps. Quart. J. R. Met. Soc., 111, 877-946.



- |   |      |   |
|---|------|---|
| Huber-Pock, F and Kress, C                              | 1981 | Contributions to the problem of numerical frontal analysis. Vienna, Zentralanst. Met-Geodyn., Pub. Nr. 253, 85-88.  |
| Monk, G A   | 1986 | The structure and evolution of split fronts. Observations of a split front: 11 April 1985. Met O 15 International Report No. 63, Meteorological Office, Bracknell.                    |
| Morris, R M   | 1971 | A case study of the spectacular developments and movement of a February storm. Met. Mag., 100, 14-27.   |
| Uccellini, L W, Keyser, D,<br>Brill, K F, and Wash, C H | 1985 | The Presidents' Day cyclone of 18-19 February 1979: Influence of upstream trough amplification and associated tropopause folding on rapid cyclogenesis. Mon. Wea. Rev., 113, 962-988. |

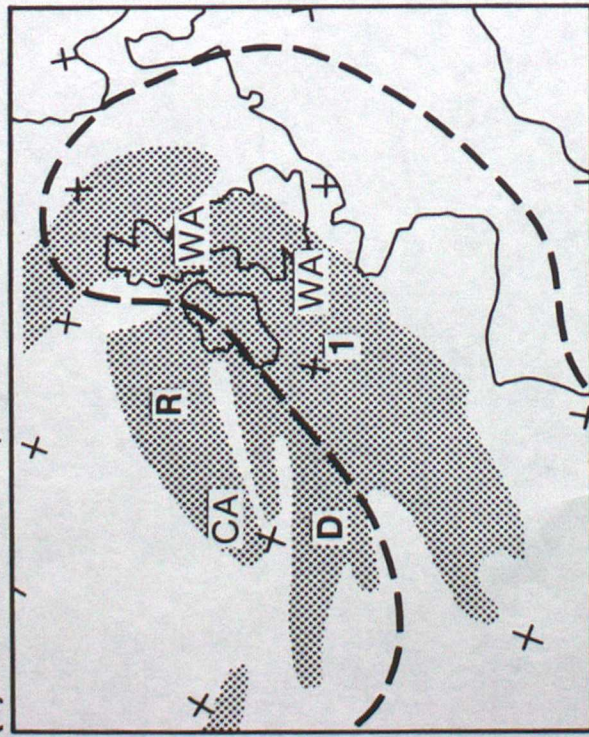


- Woodroffe, A 1984 Short-range weather forecasting  
- a current assessment.  
Bracknell, R. Met. Soc.  
Weather, 39, 1984, 298-310.
- Young, M V, Monk, G A, Browning, K A 1986 Interpretation of satellite  
imagery in a rapidly deepening  
cyclone.  
Submitted to Quart. J. R. Met.  
Soc.
- Zwatz-Meise, V, and Hailzl, G 1983 A cloud formation process  
contradictory to the classical  
occlusion development  
investigated with satellite  
images and model output  
parameters.  
Arch. Met. Biocl., Ser. A, 32,  
119-127.

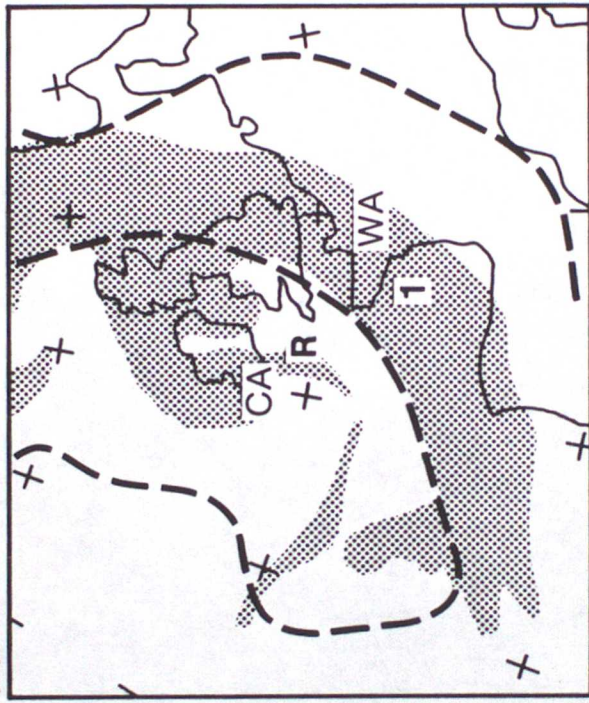


**Figure 1**

(a) 00 GMT 11 April 1985



(b) 06 GMT 11 April 1985



(c) 12 GMT 11 April 1985

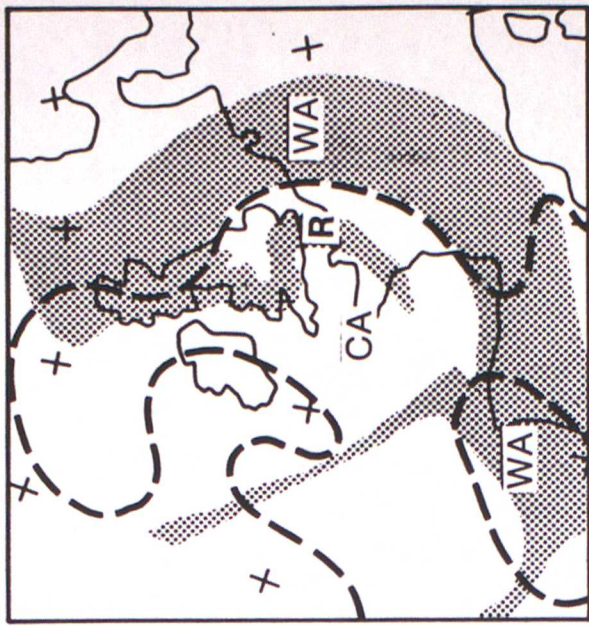
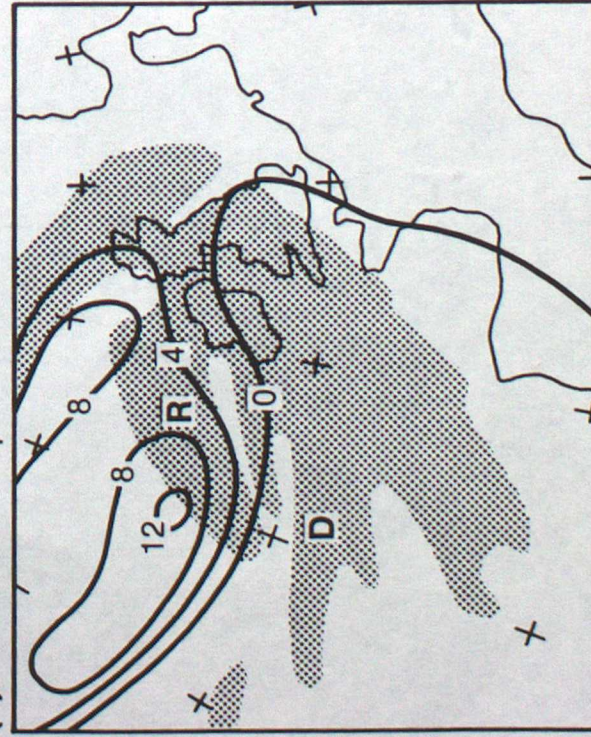


**Figure 2**

(a) 00 GMT 11 April 1985



(b) 06 GMT 11 April 1985



(c) 12 GMT 11 April 1985

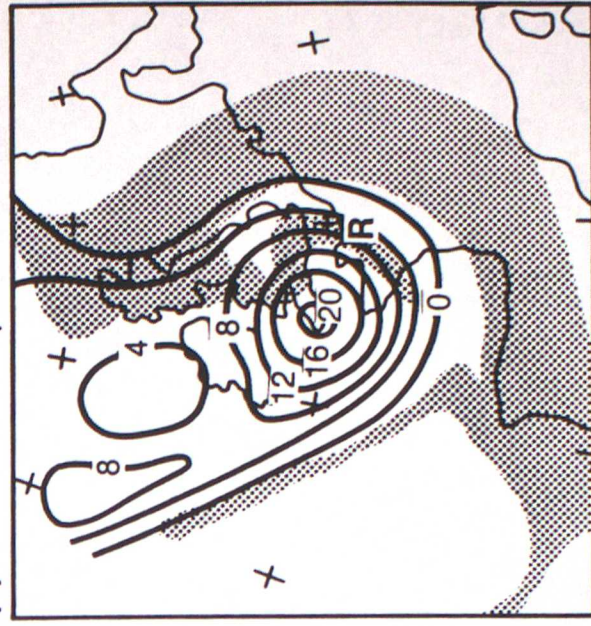
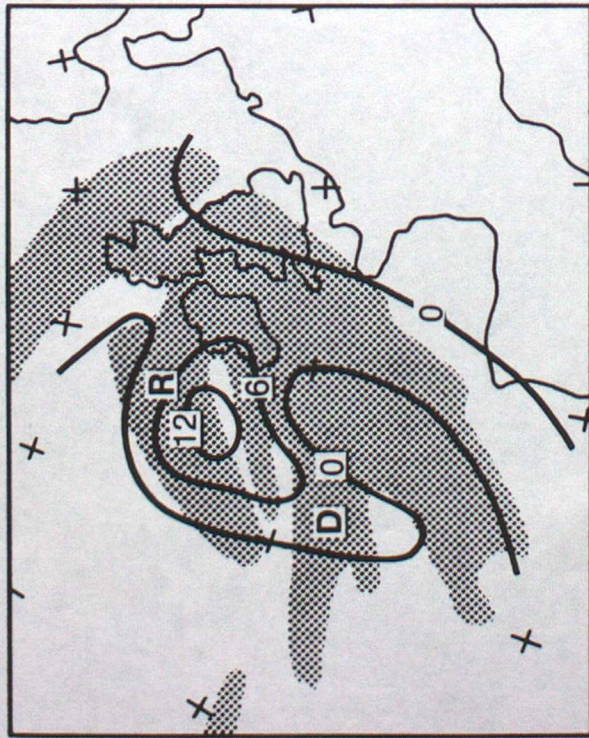




**Figure 3**

(a) 00 GMT 11 April 1985



(b) 12 GMT 11 April 1985

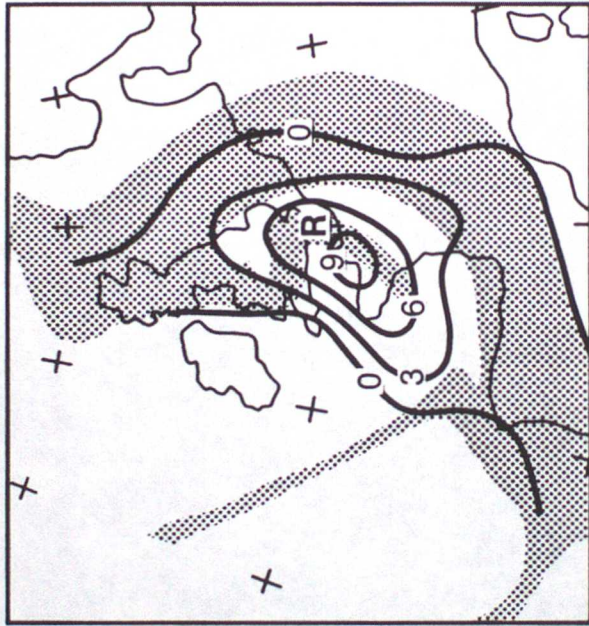
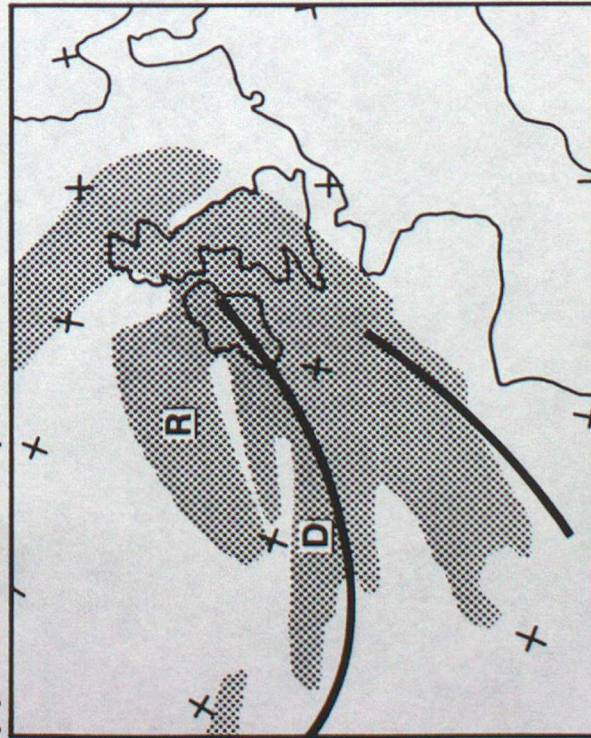


**Figure 4**

(a) 00 GMT 11 April 1985



(b) 06 GMT 11 April 1985



(c) 12 GMT 11 April 1985

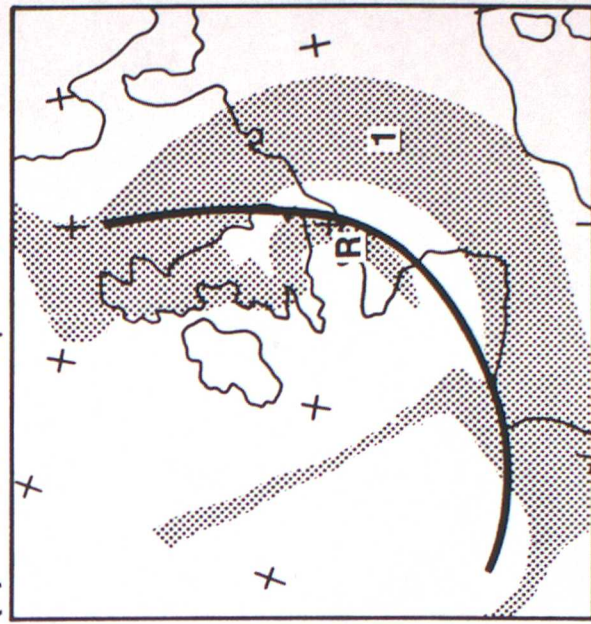




**Figure 5** T+0 00 GMT 11 April 1985

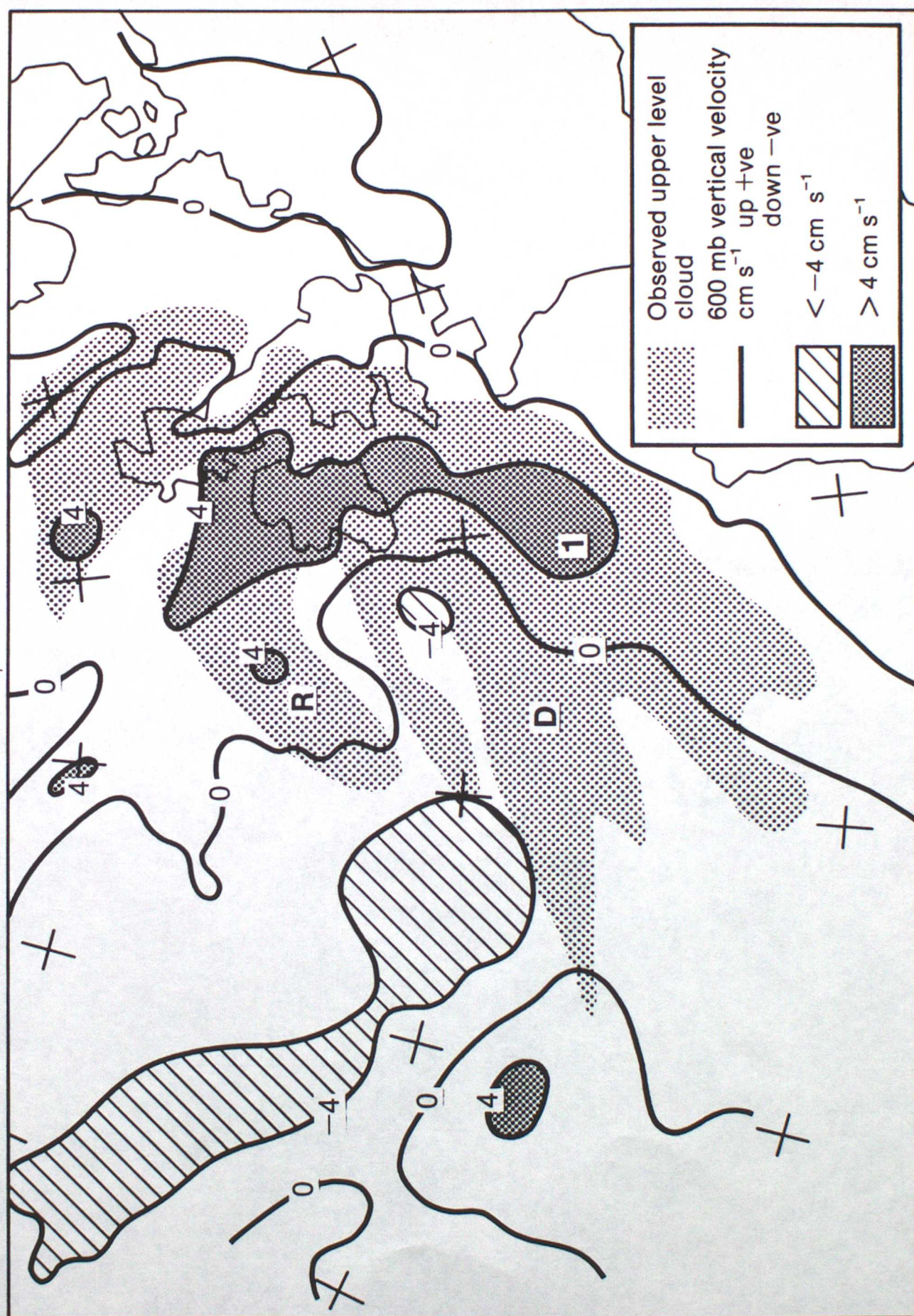
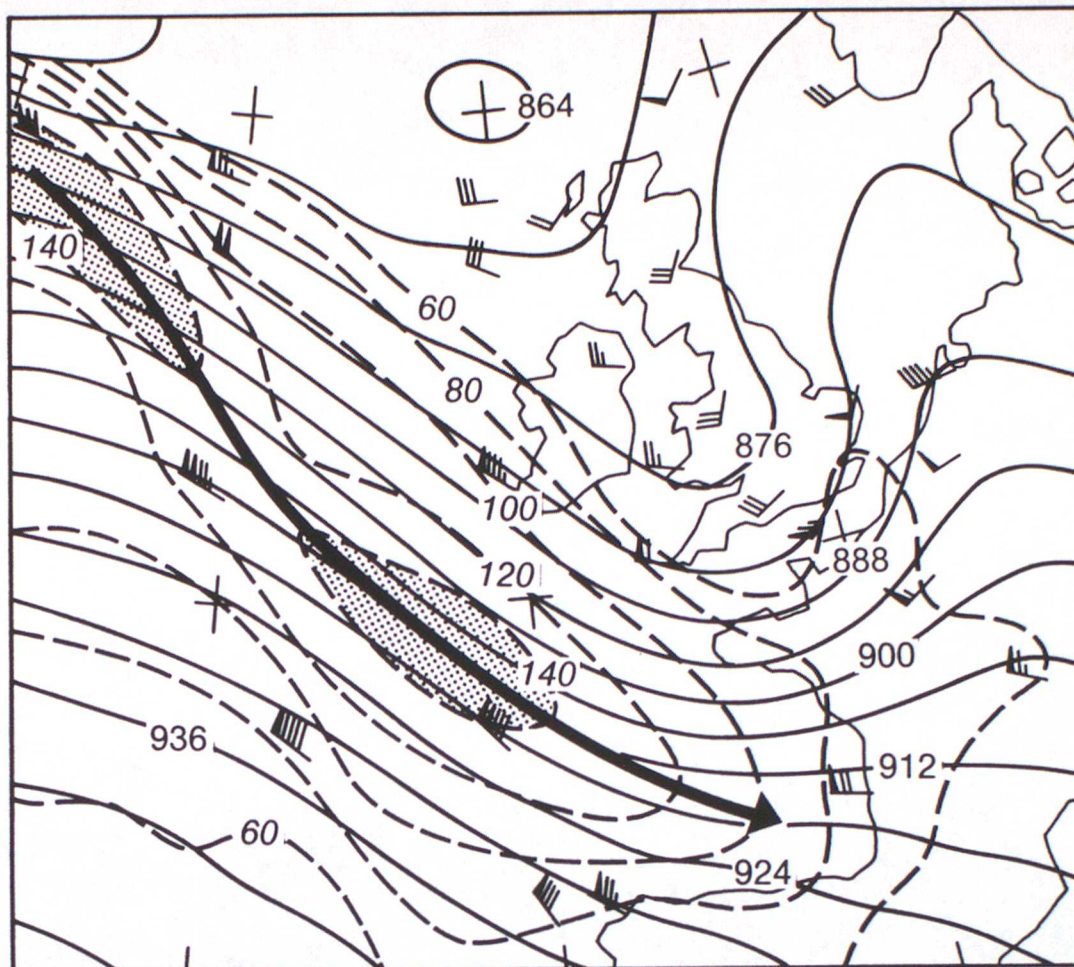




**Figure 6 (a) Analysis**

300 mb 12 GMT 11 April 1985



**(b) 24 hour fine mesh forecast**

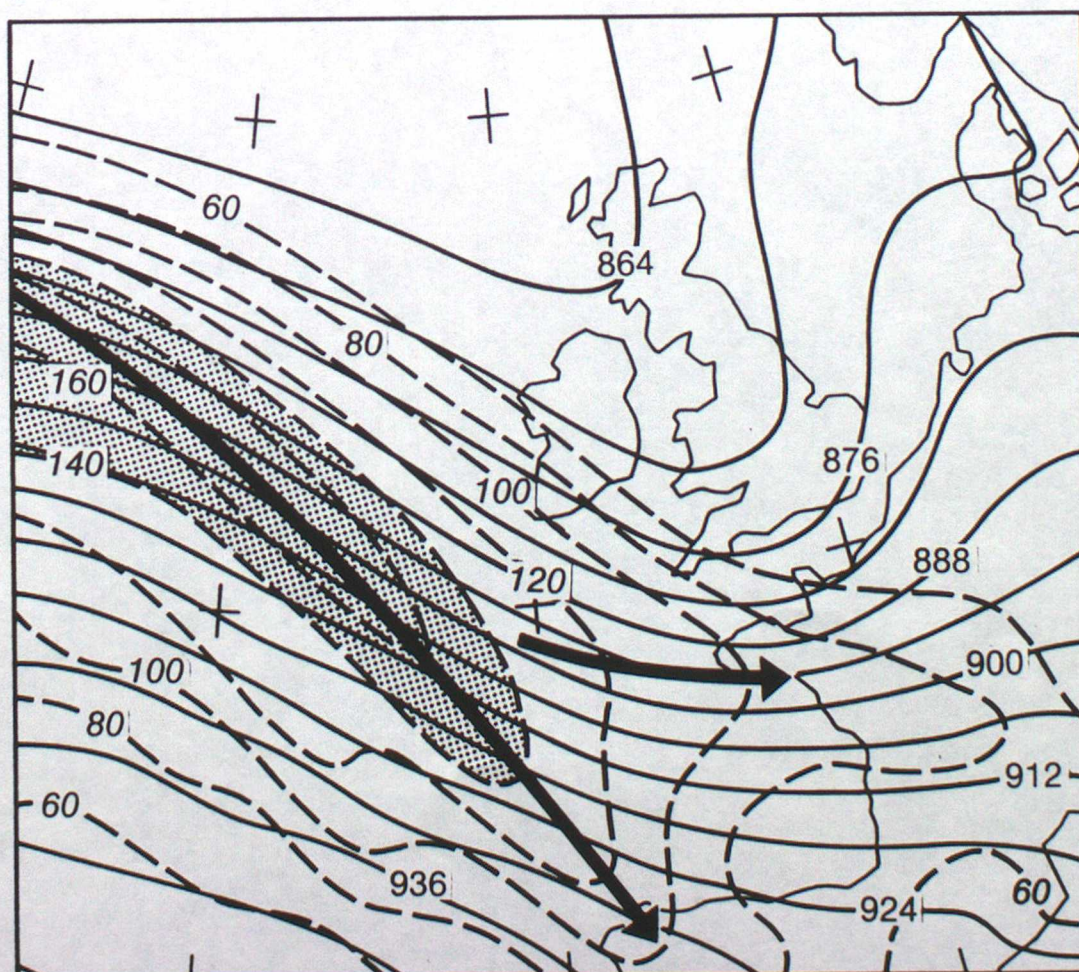




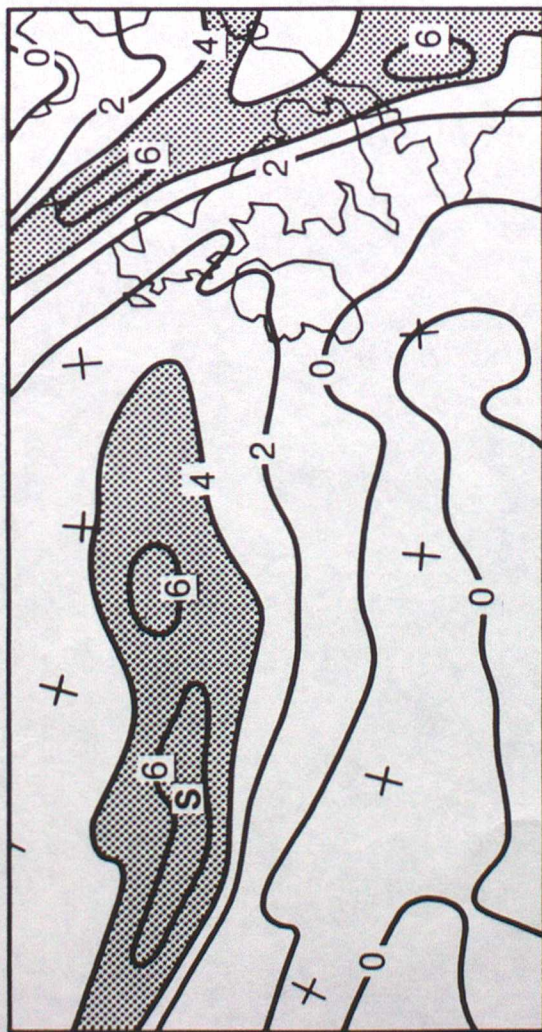
Figure 7



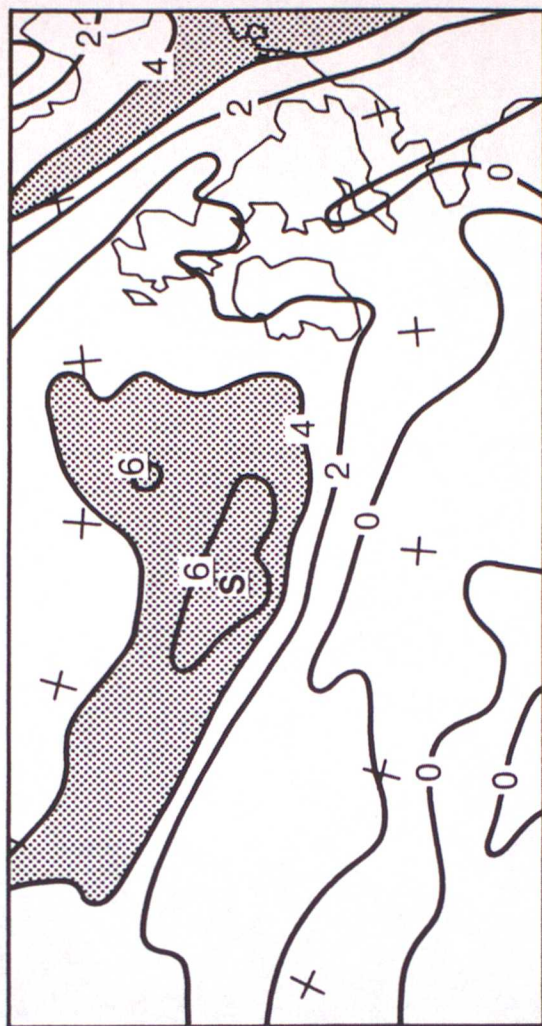


**Figure 8**

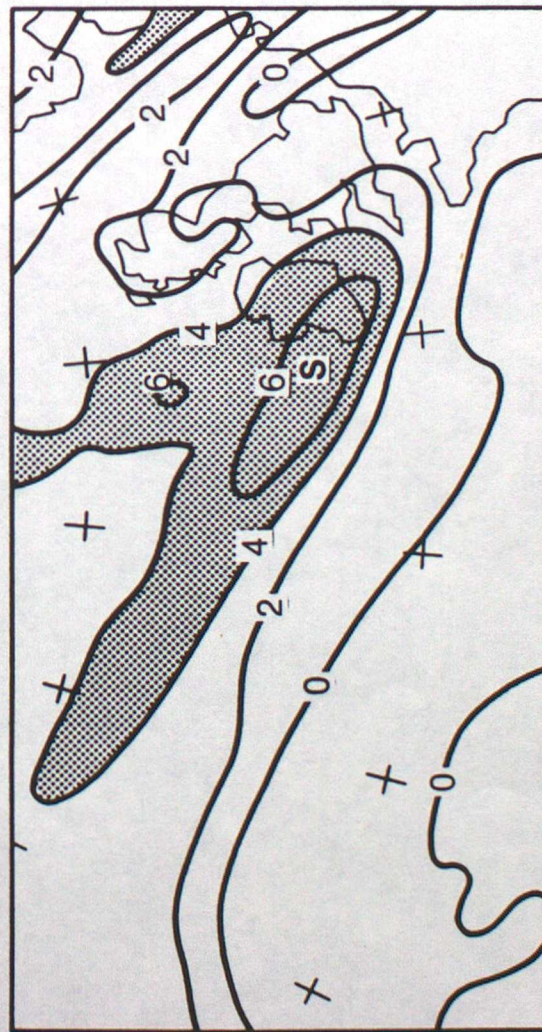
(a) T+6 18 GMT 10 April 1985



(b) T+12 00 GMT 11 April 1985



(c) T+18 06 GMT 11 April 1985



(d) T+24 12 GMT 11 April 1985

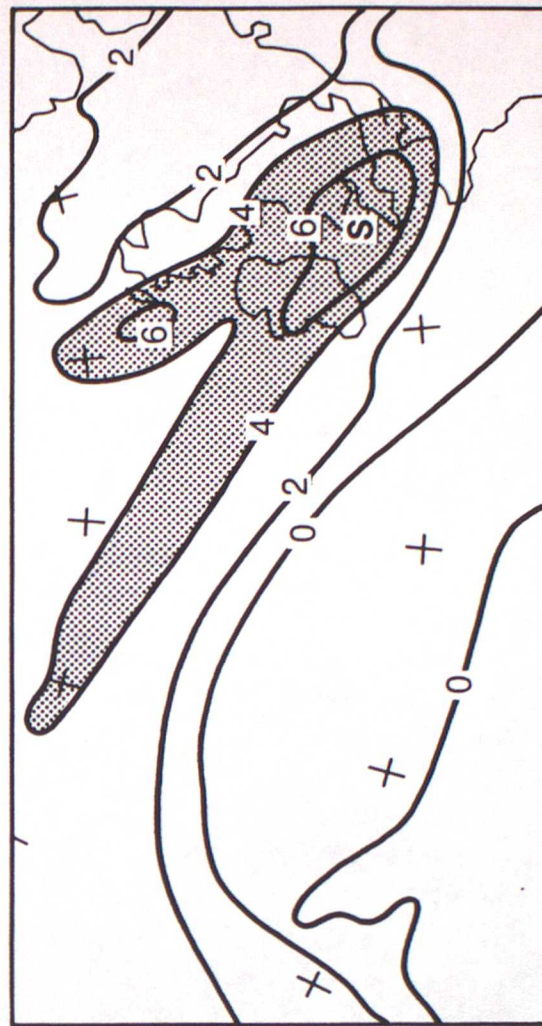




**Figure 9(a)** 12 GMT 10 April 1985

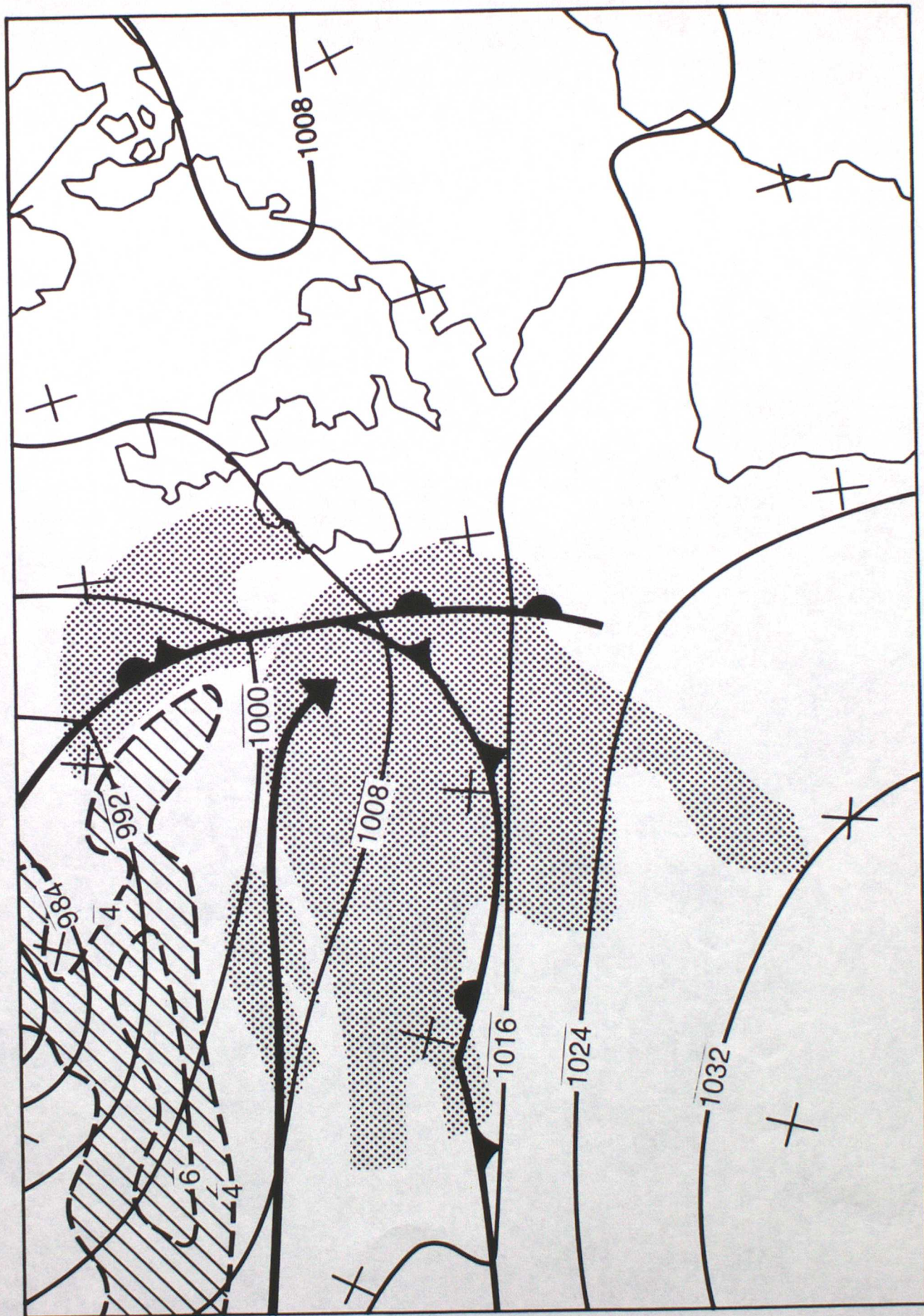




Figure 9(b) 00 GMT 11 April 1985

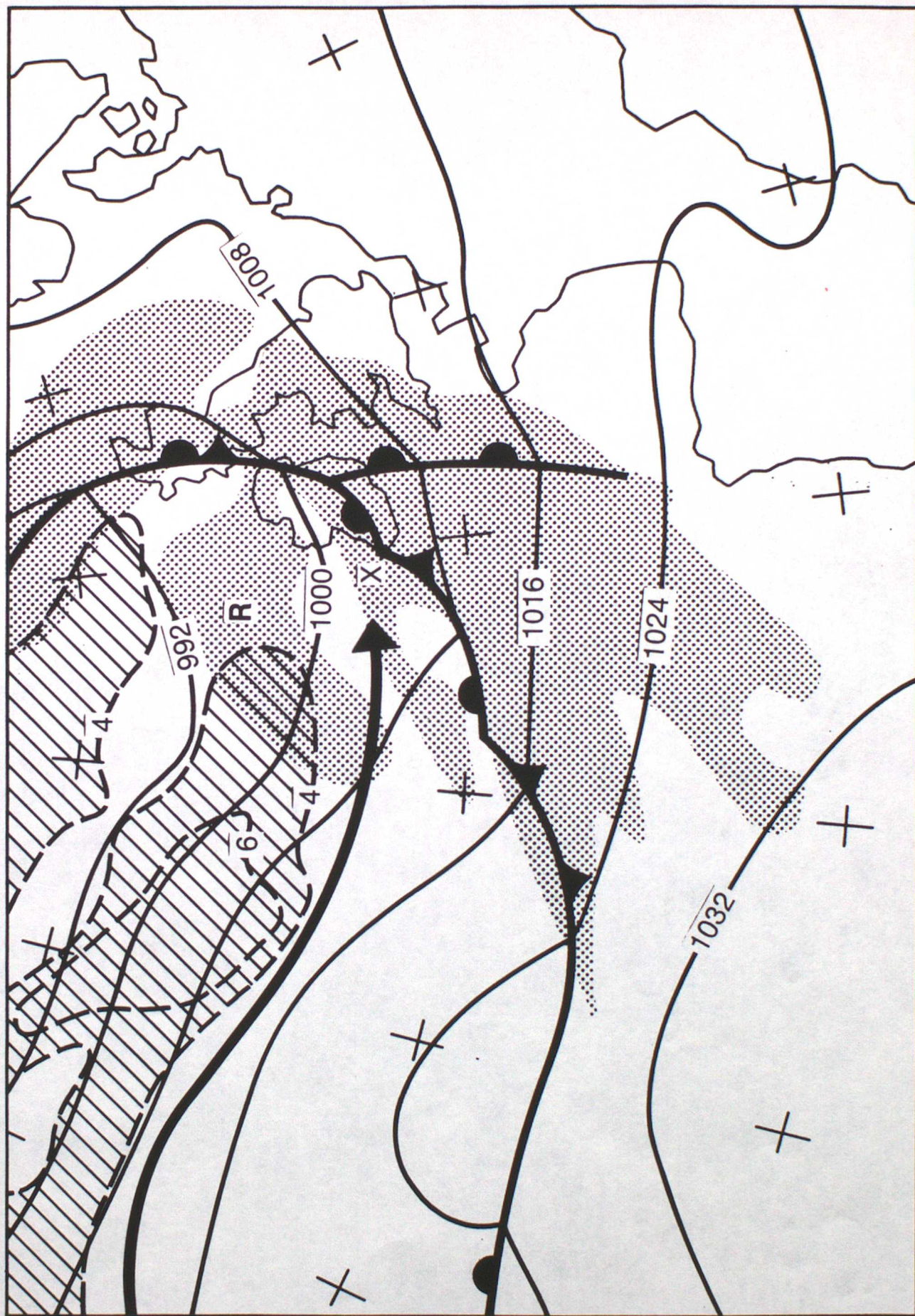
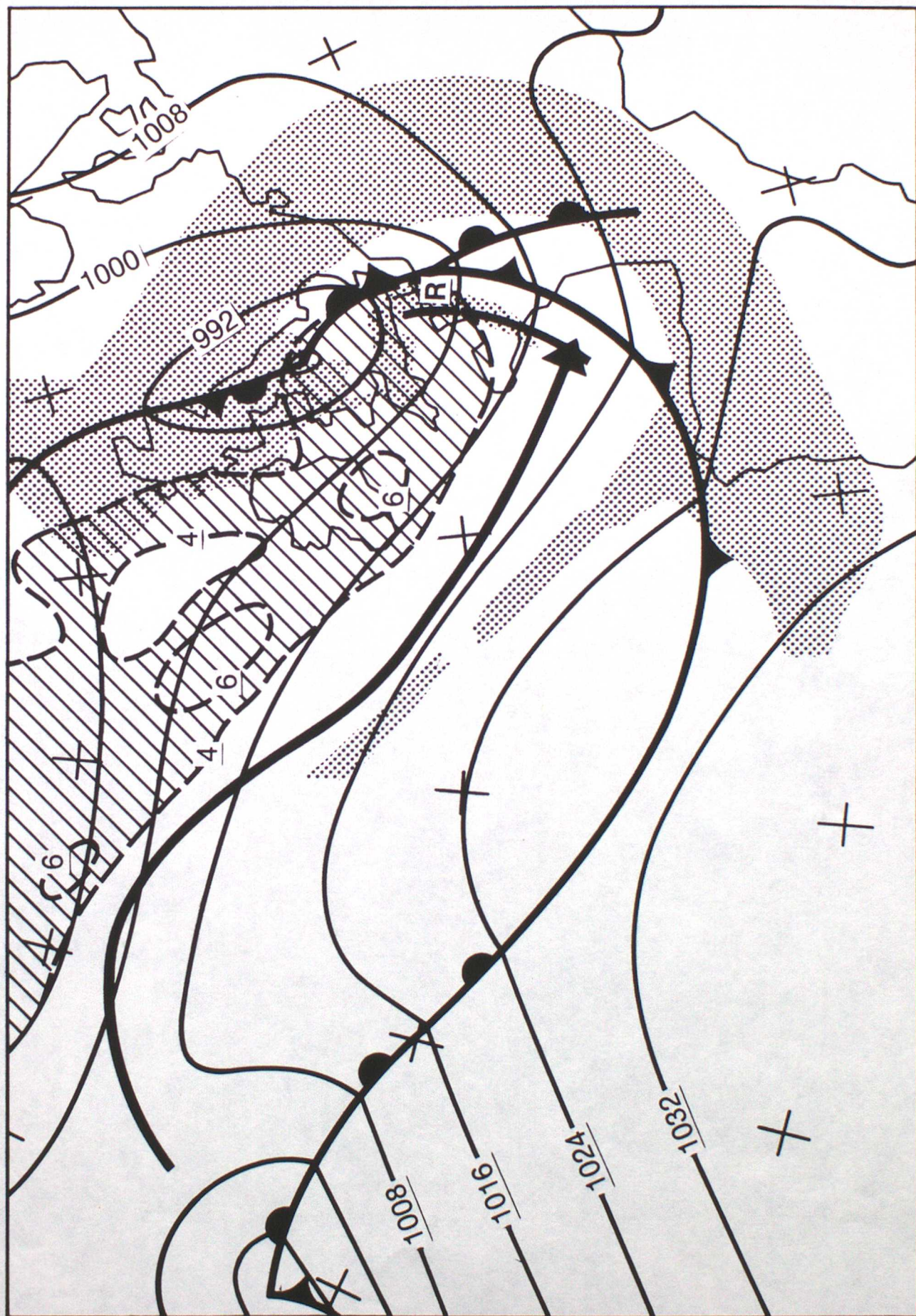




Figure 9(c) 12 GMT 11 April 1985





**Figure 10**

T+0 00 GMT 11 April 1985

$\theta = 310$

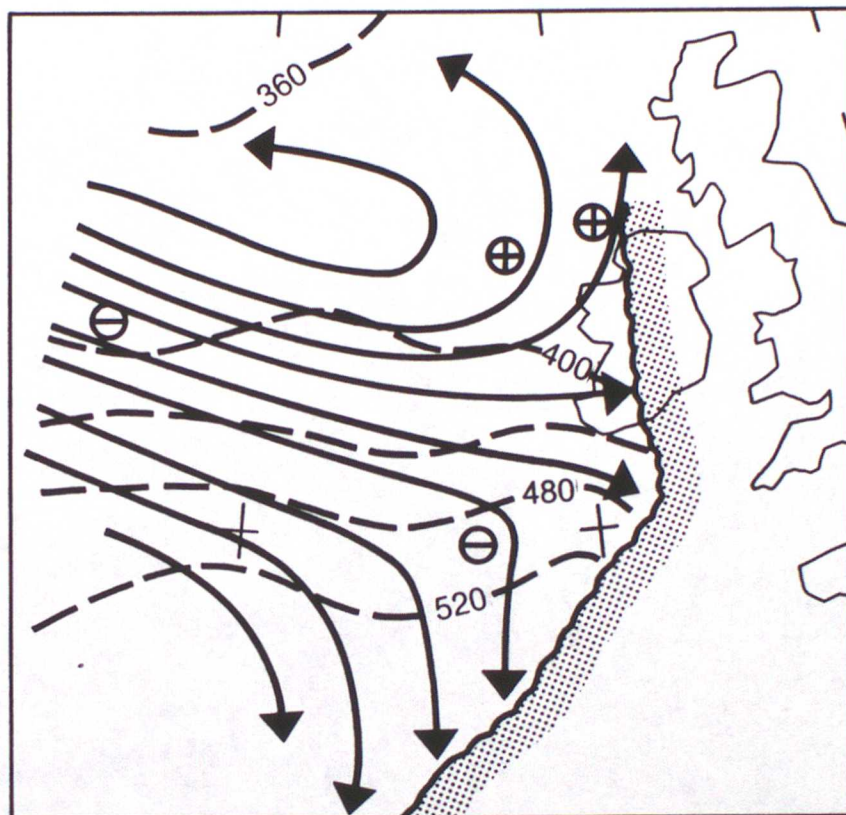




Figure 11

